

Water and other volatile systematics of olivine-hosted melt inclusions from the Yellowstone hotspot track

C. J. Stefano · S. B. Mukasa · A. Andronikov ·
W. P. Leeman

Received: 4 January 2010 / Accepted: 29 June 2010 / Published online: 13 July 2010
© Springer-Verlag 2010

Abstract Major oxide, trace element and volatile (H₂O, CO₂, S, F, and Cl) compositions have been analyzed for olivine-hosted melt inclusions in eight basalt samples from Yellowstone National Park and the Snake River Plain (SRP) to identify the least differentiated melt compositions and assess the volatile budget of the Yellowstone hotspot. Melt-inclusion chemistry was evaluated to understand potential overprinting effects in the shallow mantle and crust of magmas derived from deeper levels. Maximum water concentrations of 3.3 wt% and CO₂ up to 1,677 ppm have been observed in olivine-hosted melt inclusions from the Gerritt Basalts at Mesa Falls, Idaho (SRP region), which is significantly higher than the maximum concentrations measured in lavas from other hotspots such as Hawaii (~0.8–0.9 wt%). Maximum water concentrations were generally observed in the least differentiated melt inclusions in terms of incompatible major oxide concentrations, indicating that high water concentrations are characteristic of the mantle or perhaps lower crust rather

than resulting from differentiation enhancement within the shallow crust, even taking into account the fact that water behaves as an incompatible element during crystal fractionation. Enrichment in Ba coupled with depletion in Th in many of the melt inclusions and their host rocks is a characteristic of many arc lavas and may indicate that volatiles in Yellowstone-Snake River Plain basalts could have a subduction zone origin.

Keywords Snake River Plain · Olivine-hosted melt inclusions · Volatiles · Hotspots · Yellowstone

Introduction

The Yellowstone-Snake River Plain (YSRP) volcanic province is widely considered to be a manifestation of a hotspot that penetrates North American continental lithosphere proximal to a convergent boundary with the Juan de Fuca Plate (cf. Manea et al. 2009). While some have expressed doubt about a mantle plume origin for the YSRP volcanic province (e.g., Christiansen et al. 2002), many others have presented evidence suggestive of such an origin (e.g., Craig et al. 1978; Jordan et al. 2004; Nash et al. 2006). Some studies have explored the detailed petrogenetic processes resulting in this magmatism (cf. Leeman et al. 2008; Leeman et al. 2009; McCurry and Rogers 2009), but critical to such endeavors is knowledge of the magmatic volatile contents.

YSRP magmatism is characterized by bimodal volcanism, consisting of an early sequence of rhyolitic lavas and caldera-forming ignimbrites. These packages are associated with discrete eruptive centers, each lasting a few million years. They are followed by predominantly basaltic volcanism that buries the calderas (Leeman 1982; Christiansen

Communicated by T. L. Grove.

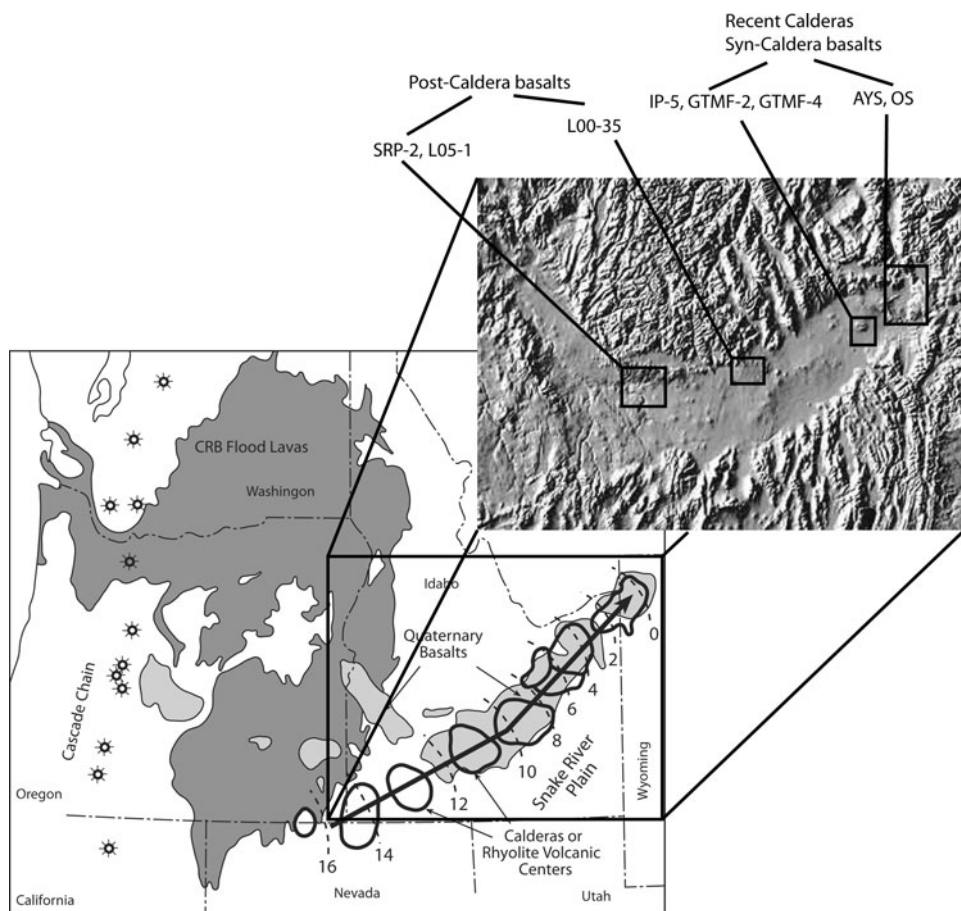
Electronic supplementary material The online version of this article (doi:10.1007/s00410-010-0553-8) contains supplementary material, which is available to authorized users.

C. J. Stefano (✉) · S. B. Mukasa
Department of Geological Sciences, University of Michigan,
Ann Arbor, MI 48109, USA
e-mail: stefanoc@umich.edu

A. Andronikov
Lunar and Planetary Laboratory, University of Arizona,
Tucson, AZ 85705, USA

W. P. Leeman
Division of Earth Sciences, National Science Foundation,
4201 Wilson Blvd., Arlington, VA 22230, USA

Fig. 1 Schematic map of the Pacific Northwest region of the United States showing the locations of the Columbia River Basalts (CRB) and the Snake River Plain (SRP). Approximate caldera locations and ages (in Ma) are shown along the Snake River Plain. Also shown is the Cascade arc. The inset shows a DEM of the SRP and the general sample locations for samples used in this study. Modified from Camp and Ross (2004)



2001; Shervais et al. 2006). Initiation of silicic magmatism was age transgressive from SW (McDermitt Caldera, ~16 Ma) to NE (Yellowstone Caldera, ~0.6 Ma), over a distance of some 700 km. The migration rate for these eruptive centers is comparable to the absolute movement of the North American Plate (~3–4 cm per year) relative to a hotspot frame of reference (Gripp and Gordon 2002), and has been discussed in detail elsewhere (cf. Leeman 1982; Pierce and Morgan 1992) (Fig. 1). Magmatism is interpreted to have commenced shortly following arrival of the plume head at the base of the lithosphere at ~17 Ma, triggering eruption of the voluminous Columbia River Flood Basalts (Carlson 1984; Hart 1985; Geist and Richards 1993; Camp 1995; Dodson et al. 1997; Camp and Ross 2004). However, density-filtering effects of thick cratonic crust/lithosphere beneath much of southern Idaho promoted intrusion rather than eruption of early basaltic magmas, and rhyolitic volcanism is interpreted to result largely from crustal anatexis in response to this process (Bonnichsen et al. 2008; Leeman et al. 2008). Based on Nd and Hf isotopic compositions and other geochemical data as much as 30–40% of the rhyolite volume could be of mantle origin (e.g., via reprocessing of early-intruded basaltic magma (Nash et al. 2006; Leeman et al. 2008; McCurry and Rogers

2009). Thus, YSRP basaltic magmatism appears to fundamentally drive the entire petrogenetic cycle from its beginning. Elevated $^3\text{He}/^4\text{He}$ ratios up to 16 R_A in YSRP basalts (Craig et al. 1978; Craig 1993; Graham et al. 2009) provide the most compelling evidence that these magmas may have a sublithospheric mantle plume source as proposed for many oceanic island basalts. However, a cratonized lithosphere source cannot be entirely ruled out if ^3He is stored in the deep crust as has been suggested for the Michigan Basin by Castro et al. (2009).

The presence of a low-velocity anomaly beneath Yellowstone extending to a depth of 500–600 km (Yuan and Dueker 2005), has been interpreted as the manifestation of a rising plume elevated in temperature relative to the ambient mantle. However, the presence of a thick lithosphere lid might prevent decompression melting of ascending plume mantle (Manea et al. 2009). Because the YSRP province transects Basin and Range structures that are observed south and north of the SRP (Leeman 1982; Nash et al. 2006), it is conceivable that YSRP basaltic volcanism is at least partly a consequence of regional extension (Bonnichsen et al. 2008; Leeman et al. 2008; cf. Harry and Leeman 1995)—perhaps abetted by an upwelling mantle plume (e.g., to account for the heat required to

produce anomalous magmatic volumes). On the other hand, Leeman et al. (2009) note petrogenetic, geochemical, and tomographic data that point to derivation of YSRP basalts from shallow (lithospheric mantle) sources that are not unusually hot, in which case, the presence of relatively fertile or hydrated mantle sources might explain the voluminous melt productivity associated with this province.

Further development of petrogenetic models for SRPY basaltic magmas will hinge on knowledge of their volatile contents. Yet, few data exist to constrain the volatile budget of hotspot basalts worldwide and none are available in continental settings. Because of the chemical heterogeneity observed in all hotspots (e.g., Weaver 1991; Kovalenko et al. 2007), it should be expected that the volatiles are also heterogeneous both in absolute concentration and relative proportions. The YSRP track is particularly interesting because the associated continental lithosphere had a protracted and complex kinematic and volcanic history prior to the presumed plume impingement against the lithosphere. For example, volatile concentrations in the YSRP magmatic systems could be elevated relative to other hotspots because of the history of subduction and arc volcanism along the Pacific margin of the North American Plate, not far from our study area when Basin and Range extension is palinspastically removed from the current lithospheric configuration.

Ideally, basalts closely related in age to the early silicic eruptive centers are likely to provide the most direct constraints on the volatile budget of the mantle source. If the source is lithospheric mantle, then over time, we would expect it to become progressively depleted in volatile components via melt extraction. Conversely, if the source is ascending plume mantle, then there may be little change in volatile content over time as source material would be continually replaced. Unfortunately, as previously noted, the earliest basaltic magmas in the YSRP system rarely erupted and direct samples are unavailable. Basaltic lavas that erupted immediately following the initial rhyolite magmatism tend to be somewhat differentiated. Many exhibit strong evidence of interaction with the crust, suggesting that they may be modified significantly during storage at crustal levels (Leeman 1982). Although this is the case for most Yellowstone basalts, relatively primitive examples do occur in the western reaches of the Yellowstone caldera system (Hildreth et al. 1991; Leeman, unpublished data). Two examples (among the most primitive YSRP basalts discussed by Leeman et al. 2009) were selected for study to assess volatile contents in the earliest available basaltic magmas in that eruptive center; these have Mg#s greater than 60 and some contain more than 10% MgO. For convenience, these lavas are designated as ‘syn-caldera’ although strictly they post-date the majority of silicic magmatism in this system.

For comparison, several basalts from the central Snake River Plain were selected for study to evaluate temporal and spatial variations in volatile budgets. These basalts have lower Mg# (52–55) and MgO (>7%) than the previously described samples, but are among the most primitive lavas available in the area. They post-date the local silicic magmatic phase by ca. 10 Ma, and are referred to in this paper as ‘post-caldera’ basalts. The use of ‘syn-caldera’ and ‘post-caldera’ is a simplification because many of caldera complexes are not well defined and, in fact, their locations are inferred from the distribution of rhyolite lavas and tuffs. However, we have chosen these terms because they provide the simplest way to define the relative timing of eruption between the studied basalts and associated rhyolitic eruptive centers. Basic information on all samples studied, including their bulk compositions, is provided in Table 1.

Olivine-hosted melt inclusions arguably provide the most direct means measuring pre-eruptive volatile contents of basaltic magmas, potentially constraining source volatile contents, and perhaps elucidating the operative melting processes (Danyushevsky et al. 2002; Hauri 2002; Wallace 2005, Kent 2008). These objectives often are hampered by a number of factors. One universal limitation is that melt inclusions are trapped at depths over which olivine is a liquidus phase. Based on direct experiments (Thompson 1975), this is the case for SRP basalts at pressures below ca. 0.8–1.0 GPa, so the melt inclusions cannot record details of magma evolution under deep crust or mantle conditions. In other words, at best, trapped melt inclusions are likely to provide only minimal estimates of magmatic volatile contents due to degassing effects prior to melt entrapment. Furthermore, melt inclusions may be modified to some extent by interaction with the host olivine and by post-entrapment crystallization (PEC). This is a prevalent issue in the SRPY province because rapidly quenched scoreacious tephra that best preserve glassy primary melt inclusions (e.g., Luhr 2001; Sadofsky et al. 2008) are rarely available for the most primitive SRPY basalts. Our work necessarily utilized subaerial lavas and the melt inclusions typically consisting of glass ± gas bubbles ± daughter minerals; homogeneous inclusions are rare. Prior to being analyzed, such inclusions must be rehomogenized at close to magmatic temperatures, then quenched to produce homogeneous glasses (Danyushevsky et al. 2002; Kent 2008). Because volatile solubility in magmas increases with pressure (Moore et al. 1998), in this study, rehomogenization was performed at elevated pressure (~6 kbar). This approach minimizes the possibility of melt-inclusion rupture and volatile losses.

This paper primarily reports the results of Fourier transform infrared (FTIR) spectroscopy, electron microprobe (EMP), secondary ion mass spectrometer (SIMS),

Table 1 Samples analyzed

Sample #	Syn-Caldera					Post-Caldera		
	GTMF-2	GTMF-4	IP-5	AYS	OS	L05-1	L00-35	SRP-2
Age (Ma)	0.2	0.2	<0.6	<0.6	<0.6	<1	1	<1
Setting	Gerritt basalt near Mesa Falls	Gerritt basalt near Mesa Falls	Spencer-Kilgore Lava Field	Osprey Basalt AYS-29-05 in Christiansen 2001	Osprey Basalt 9YC-514 in Christiansen 2001	Late SRP basalt	Late SRP basalt	McKinney Basalt, late SRP basalt
SiO ₂	48.26	48.41	48.12	52.88	50.35	2.21	2.39	2.96
TiO ₂	1.58	1.57	1.20	1.94	1.59	16.22	15.55	14.85
Al ₂ O ₃	15.65	16.28	14.63	14.81	15.34	11.21	11.94	13.37
FeO	10.58	10.37	11.60	11.89	11.67	0.18	0.19	0.20
MnO	0.18	0.18	0.18	0.17	0.16	7.59	7.31	7.64
MgO	9.44	8.68	10.59	5.83	8.18	9.92	10.09	9.10
CaO	11.32	11.57	10.90	9.69	10.59	2.84	2.59	2.64
Na ₂ O	2.34	2.36	2.13	2.81	2.55	0.66	0.80	0.72
K ₂ O	0.45	0.42	0.36	0.79	0.54	0.28	0.22	0.18
P ₂ O ₅	0.20	0.15	0.28	0.24	0.19			
Rb	8.1	7.2	6.7			12.8	16.4	14.0
Sr	215	218	174			334	331	311
Y	21.6	19.3	23.4			22.3	21.0	23.5
Zr	125	123	109			202	172	226
Nb	12.6	12.3	10.1			19.4	15.3	18.6
Ba	229	227	186			386	396	368
La	10.73	9.26	11.30			13.67	11.88	12.93
Ce	23.26	19.94	22.40			29.17	25.57	27.50
Pr	3.09	2.69	2.88			3.84	3.45	3.64
Nd	13.62	11.81	12.80			16.74	15.18	15.97
Sm	3.50	3.13	3.52			4.10	3.89	4.11
Eu	1.37	1.31	1.26			1.76	1.79	1.96
Gd	3.96	3.52	3.74			4.38	4.15	4.46
Dy	4.26	3.92	4.34			4.50	4.31	4.79
Er	2.41	2.20	2.63			2.49	2.49	2.66
Yb			2.25					
Th	0.66	0.62	0.72			1.26	1.50	1.77
U	0.18	0.16	0.23			0.38	0.34	0.50

Host-rock sample numbers with descriptions and major and trace element chemistry. Analyses for Osprey Basalt samples are from Christiansen 2001

and laser ablation inductively coupled plasma mass spectrometer (LA-ICP-MS) study of melt inclusions from representative olivine phenocrysts separated from these samples.

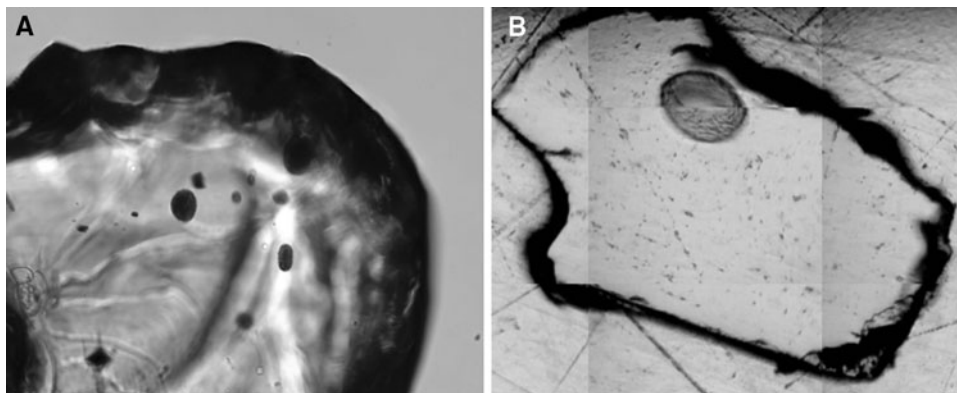
Methods for the preparation and homogenization of olivine-hosted melt inclusions

Sample selection and homogenization

Seventy-six olivine grains 425 μm to 1 mm in size were separated from eight basalt samples and individually

inspected under the binocular microscope to identify melt inclusions, which invariably appeared crystalline. Equant-shaped melt inclusions with diameters greater than 50 μm length were handpicked for analysis. Olivine grains displaying internal fracturing or alteration were discarded to avoid secondary effects and the possibility of volatiles being introduced into the melt inclusions from outside the olivine grains. Representative images of unhomogenized, homogenized, and polished melt inclusions used in this study are shown in Fig. 2. Homogenization of melt inclusions was achieved in the High Pressure Laboratory at the University of Michigan using the piston cylinder apparatus (see Hui et al. (2008) for calibration). Between 10 and 15

Fig. 2 Representative examples of olivine-hosted melt inclusions used in this study. **a** An olivine grain with several inclusions to 50 μm prior to homogenization. **b** A homogenized and doubly polished 70- μm inclusion



olivine grains were packed in graphite powder inside a single graphite capsule and were then brought to temperature and pressure in the piston cylinder apparatus to achieve homogenization, using a barium carbonate pressure medium for heating to homogenize the melt inclusions. The charge was heated to 1,300°C at a pressure of approximately 6 kbars in less than 1 min, held there for 18–20 min, and then quenched to below 200°C within 20 s. According to work done by Zhang et al. (1989) and Chen and Zhang (2008), any quench-related modifications of inclusions under these conditions should be negligible. The temperature of 1,300°C was chosen in order to be significantly above the basalt liquidus (usually in the range of 1,100–1,200°C, depending on melt composition, including H₂O content) so that melting and homogenization are rapid to minimize volatile diffusion in or out of the inclusion before quench. These techniques were previously employed by Zhang and Stolper (1991) and Chen and Zhang (2008), and in both cases, there was no detectable change in H₂O concentration during the experiment, ruling out the possibility of H₂O addition to the melt inclusions by the experimental assembly. The olivine grains were then individually mounted in epoxy resin and then ground and polished until inclusions were exposed on both sides of the mount. Final thicknesses ranged approximately from 20 to 70 μm . Care was taken at this time to once again monitor for cracks or other signs of inclusion rupture or alteration. Any samples with cracks that intersected the targeted melt inclusions were discarded, with the exception of those cracks that developed during the final stages of polishing, as these would not allow appreciable modification in the inclusion volatile contents. Any inclusions not completely homogenized were also discarded.

Water analysis by FTIR

Polished melt inclusions were analyzed at the University of Michigan for H₂O on a Perkin Elmer Spectrum GX FTIR spectrometer microscope attachment in an environment

purged with N₂. Typical melt inclusion diameter is 50 μm , and an infrared aperture of 20 μm by 20 μm was used. The thickness of the section is measured to a precision of 1 μm . The calibration of Dixon et al. (1995) was used to calculate the H₂O concentrations from the $\sim 3,500\text{ cm}^{-1}$ absorbance peak. H₂O measurements were all reproducible to $\pm 10\%$.

Major oxide analysis for the inclusions and host-olivine grains

Major oxide concentrations for inclusions and host-olivine grains were determined on a Cameca SX100 Electron Microprobe at the University of Michigan. Measurements were made with an accelerating voltage of 15 kV, a beam current of 4 nA, and a 5- μm defocused beam. Counting times were typically 20 s, with a sub-counting routine on Na to monitor for potential beam damage to the glasses. The sub-counting routine breaks counts for Na into 5-s increments, allowing the user to note time-dependent shifts in Na count rates that would indicate beam damage to the glass. The sub-counting routine also includes an algorithm that corrects for any beam damage by calculating back to $t = 0$ for any time-dependent change in Na count rate. In none of the cases was correction necessary. Host-olivine grains were analyzed in the same way, except that a beam current of 10 nA and a point beam were used. Elemental standardization was achieved with known natural mineral samples (Albite for Na and Al, diopside for Mg, Si and Ca, adularia for K, imenite for Ti, rhodonite for Mn, ferrosilite for Fe, apatite for P). Major oxides other than MnO and P₂O₅ were reproducible to $\pm 1\%$.

Volatile- and trace-element analysis of the inclusions by SIMS and LA-ICP-MS

Selected melt inclusions from each sample were analyzed for H₂O, F, Cl, and S using a 10- μm Cs⁺ ion beam on the Cameca 1280 SIMS at the Woods Hole Oceanographic

Institution following the method described in Le Voyer (2008). Additionally, four melt inclusions from sample GTMF-4, a Gerrit Basalt, were analyzed for CO₂. A set of volatile-rich basaltic glasses (0.1–6.5% H₂O) was used for the calibration. SIMS data were reproducible to ±1%. We observed no systematic difference between the FTIR and SIMS data for inclusions with lower water concentrations (<1.5 wt%), whereas SIMS gave systematically higher water concentrations for the more water-rich inclusions, the discrepancy increasing with increasing concentration (2.5 wt% vs. 3.5 wt% in the most water-rich inclusion in this study). This discrepancy is attributed to potential detector saturation in the FT-IR instrument. Although peaks do not appear to show “flattening” associated with saturation, repolishing inclusions to thinner wafers could often cause measured water concentration to increase, supporting the notion that detector saturation is responsible for this discrepancy. Consequently, we have opted to report SIMS data for the inclusions with higher water concentrations over FTIR data when available.

A subset of 54 inclusions was analyzed for selected trace elements (Sc, Rb, Sr, Y, Zr, Nb, Ba, La, Ce, Pr, Nd, Sm, Eu, Gd, Dy, Er, Yb, Th, and U) using the laser ablation inductively coupled plasma mass spectrometer (LA-ICP-MS) at Oregon State University. Ablation was achieved using a NewWave DUV 193 ArF Excimer laser, and analysis was performed on a VG ExCell quadrupole ICP-MS. The laser spot size was 50 μm, and the pulse rate was set to 4 Hz. Analyses were calibrated using the ⁴³Ca peak in the sample, while regularly monitoring the BCR-2G and BHVO-2G glass standards, as detailed by Kent et al. (2004). Based on repeated standard analysis, all trace elements were reproducible to ±10% or better.

Host-rock analysis

Major oxides and the trace elements Rb, Sr, and Zr for the bulk rock lavas were analyzed by X-ray fluorescence (XRF), and other trace elements were measured by LA-ICP-MS at the XRF and ICP-HEX-MS Laboratories of the Washington State University Geoanalytical Laboratory following the methods of Knaack et al. (1994) and Johnson et al. (1999).

Results

Major oxide, as well as trace element and volatile data for olivine-hosted melt inclusions and their associated whole rocks from eight basalt flows throughout the Snake River Plain are presented in Tables 1 and 2. The five samples associated with the current Yellowstone-Island Park caldera complex (Fig. 1) are considered to be syn-caldera

basalts and are all younger than the Lava Creek Tuff (0.6 Ma). The other three flows, from the central SRP, are much younger than the nearest caldera and are considered to be post-caldera.

Olivine compositions

Host-olivine compositions for the syn-caldera melt inclusions show a range of ~Fo_{84–87} (host rock Mg#s range from 47 to 62). The post-caldera olivine grains are generally less magnesian, but are more heterogeneous, with a range of ~Fo_{69–82} (host rocks Mg#s range from 50 to 55). Forsterite contents in individual samples do not generally vary by more than 3 wt% (the exception being post-caldera sample L05-1, showing as much as 11 wt%) and do not correlate with water.

Major element compositions of the melt inclusions

Major oxide data for both syn-caldera and post-caldera melt inclusions display compositional trends, despite some scatter. When melt inclusion compositions are plotted against the compositions of suites of whole rocks from the same area taken from the literature (Fig. 3), they are found to follow the compositional trends defined by those rocks, although they tend to extend those trends to less differentiated compositions. They also tend to show broader scatter about those trends, probably representing a combination of potential source heterogeneity, small-scale crystallization/contamination effects and the higher uncertainties associated with the analysis of the inclusions as opposed to the whole rocks. Iron loss is a common problem in olivine-hosted melt inclusions (Danyushevsky et al. 2002; Kent 2008). However, no melt-inclusion compositions from this study show anomalous iron concentrations when compared to whole rock suites. Overall, this consideration lends confidence that the melt inclusions are representative of their host magmas.

Most melt-inclusion and host-rock compositions fall in the basalt field on the total alkalis vs. silica diagram (Fig. 4); however, a wide variety of other compositions also occur. It is important to note at this time that these exotic compositions may represent real liquids that were present in the magma system, but may instead result from edge effects and other localized reaction effects, as discussed by Danyushevsky et al. (2004). Post-caldera melt inclusions show less heterogeneity but are more alkaline on average than the syn-caldera inclusions, although a couple of extreme alkaline compositions are observed in some syn-caldera inclusions from Yellowstone. The melt inclusions' major oxide compositions are quite variable within a given sample, but the host-rock composition in each case is within the range defined by the melt

Table 2 Selected data for olivine-hosted melt inclusions from the Snake River Plain

wt%	GTMF-2-2	GTMF-2-3	GTMF-2-4	GTMF-2-5	GTMF-2-6	GTMF-2-7	GTMF-2-9	GTMF-2-10	GTMF-2-11	GTMF-2-12
SiO ₂	47.34	47.22	47.69	47.05	44.36	45.99	47.31	44.83	45.49	46.33
TiO ₂	1.59	1.45	2.20	1.52	1.78	1.31	1.78	1.29	1.31	0.99
Al ₂ O ₃	14.51	15.35	11.55	16.46	14.19	14.98	16.64	13.68	14.69	11.98
FeO	9.70	8.30	10.71	9.43	12.51	8.43	9.63	11.06	10.59	18.13
MnO	0.21	0.13	0.19	0.14	0.23	0.18	0.14	0.16	0.19	0.31
MgO	11.72	12.50	13.16	9.76	9.63	13.21	7.65	14.01	11.89	12.73
CaO	11.12	11.64	10.19	11.76	11.30	11.32	12.41	10.43	11.08	4.98
Na ₂ O	2.37	2.19	2.40	2.09	4.01	3.41	2.70	2.74	3.34	2.97
K ₂ O	0.55	0.34	0.53	0.43	0.62	0.34	0.55	0.42	0.37	0.71
P ₂ O ₅	0.26	0.31	0.49	0.30	0.33	0.32	0.49	0.21	0.29	0.28
H ₂ O	0.63	0.56	0.89	1.07	1.04	0.52	0.71	1.17	0.78	0.58
Olivine FO		85.53			84.67					
H ₂ O								1.27		1.00
ppm										
F								401		689
S								1,369		423
Cl								182		129
Sc	30	22	39	23	25			26		
Rb	10.6	7.2	12.5	7.8	7.1			6.4		
Sr	209	201	175	194	1,284			158		
Y	23	20	31	22	22			19		
Zr	116	91	167	126	126			127		
Nb	13.2	10.3	18.3	14.1	17.6			14.6		
Ba	294	186	342	207	2,916			488		
La	14.0	9.3	18.5	11.8	8.8			7.2		
Ce	36.0	27.3	46.6	32.7	22.3			22.3		
Pr	4.2	3.2	5.6	4.1	2.9			2.6		
Nd	18.6	14.3	21.7	16.3	12.7			13.0		
Sm	4.1	4.0	4.6	4.5	3.3			3.4		
Eu	1.2	1.4	1.8	1.3	1.5			1.2		
Gd	3.6	3.7	6.1	4.2	4.2			4.8		
Dy	4.1	4.0	5.5	3.3	4.1			3.2		
Er	2.5	2.0	3.3	2.1	2.4			2.3		
Yb	2.7	1.3	4.1	1.8	2.5			2.1		
Th	0.4	0.3	0.6	0.4	0.4			0.4		
U	0.3		0.3	0.1	0.3			0.2		
wt%	GTMF-2-13	GTMF-4-3	GTMF-4-6	GTMF-4-7	GTMF-4-8	GTMF-4-20	GTMF-4-21			
SiO ₂	44.08	39.49	47.54	45.37	47.93	41.05	43.42			
TiO ₂	1.51	2.74	1.63	1.34	1.53	1.62	1.93			
Al ₂ O ₃	13.93	12.30	15.03	12.96	14.17	14.93	14.34			
FeO	11.32	14.65	9.02	10.78	10.18	15.67	12.05			
MnO	0.12	0.22	0.22	0.20	0.13	0.23	0.21			
MgO	14.09	11.22	11.07	15.73	12.41	10.21	13.50			
CaO	11.08	14.97	11.55	9.80	10.61	11.80	11.18			
Na ₂ O	2.10	2.10	2.36	1.49	1.95	1.57	0.93			
K ₂ O	0.36	0.33	0.36	0.35	0.35	0.44	0.29			
P ₂ O ₅	0.20	0.44	0.28	0.29	0.27	0.37	0.26			

Table 2 continued

wt%	GTMF-2-13	GTMF-4-3	GTMF-4-6	GTMF-4-7	GTMF-4-8	GTMF-4-20	GTMF-4-21		
H ₂ O	1.20	1.54	0.93	1.69	0.48	2.13	1.89		
olivine FO							84.91		
H ₂ O				2.00		3.30			
ppm							CO ₂		
F				362		460			
S				1,700		898			
Cl				186		1,100			
Sc	32			25	57				
Rb	5.8			5.3	6.8				
Sr	135			271	198				
Y	20			22	24				
Zr	122			131	118				
Nb	12.1			13.9	11.6				
Ba	206			2,780	205				
La	8.5			12.8	12.9				
Ce	23.0			27.1	28.9				
Pr	2.9			3.6	3.2				
Nd	12.6			15.5	17.6				
Sm	3.6			3.4	4.5				
Eu	1.0			1.4	1.3				
Gd	3.8			5.0	4.2				
Dy	2.8			4.8	3.4				
Er	2.3			2.6	2.3				
Yb	1.6			1.9	1.3				
Th	0.4			0.3	0.7				
U	0.2			0.2					
wt%	L00-35-3	L00-35-4	L00-35-6	L00-35-8	L00-35-9	L00-35-10	L00-35-11	L00-35-13	SRP-2-1
SiO ₂	47.33	43.29	48.31	45.18	47.77	47.65	47.40	47.79	44.26
TiO ₂	2.32	4.17	1.08	2.02	2.73	2.52	2.37	2.66	3.02
Al ₂ O ₃	12.81	12.20	12.12	12.53	14.28	13.48	13.29	13.00	11.92
FeO	12.00	16.55	16.90	16.79	11.17	10.71	11.19	11.95	17.25
MnO	0.26	0.28	0.41	0.26	0.21	0.17	0.26	0.24	0.27
MgO	11.25	11.87	9.22	8.57	9.00	10.63	11.26	9.08	11.18
CaO	10.02	7.93	5.18	8.62	10.13	10.45	9.93	10.89	8.21
Na ₂ O	2.39	2.04	4.80	4.41	2.69	2.55	2.48	2.56	2.33
K ₂ O	0.80	0.64	1.08	0.28	0.92	0.84	0.80	0.80	0.77
P ₂ O ₅	0.59	0.79	0.81	0.36	0.51	0.51	0.53	0.53	0.60
H ₂ O	0.23	0.24	0.08	0.98	0.58	0.48	0.49	0.50	0.21
olivine FO	78.03	79.27			78.04	78.01			73.23
H ₂ O		0.53			0.42				0.30
ppm									
F		431			55				826
S		91			173				968
Cl		541			16				70
Sc	26	38		74	26	24			30
Rb	19.5	10.2		4.6	19.1	19.5			17.0
Sr	309	281		264	309	314			263

Table 2 continued

wt%	L00-35-3	L00-35-4	L00-35-6	L00-35-8	L00-35-9	L00-35-10	L00-35-11	L00-35-13	SRP-2-1	
Y	29	39		30	27	29			31	
Zr	177	161		163	180	179			228	
Nb	18.0	21.8		15.9	17.2	18.9			22.1	
Ba	472	423		367	464	474			437	
La	20.5	27.1		23.3	20.8	20.3			24.5	
Ce	56.6	68.2		64.1	56.6	58.9			61.5	
Pr	6.3	8.6		4.7	6.8	6.7			7.5	
Nd	28.9	38.8		18.2	27.5	29.9			33.6	
Sm	6.4	9.3		5.5	4.5	6.6			5.6	
Eu	1.7	2.6		1.9	2.3	2.3			2.3	
Gd	6.2	7.7		4.1	6.3	5.0			7.4	
Dy	5.7	7.3		5.6	4.7	4.2			6.2	
Er	2.3	4.3		3.4	3.0	2.7			3.6	
Yb	2.2	4.0		1.1	1.7	2.5			3.1	
Th	1.6	1.4		1.5	1.9	1.4			1.8	
U	0.3	0.2		0.6	0.5	0.3			0.7	
wt%	SRP-2-3	SRP-2-4	SRP-2-5	SRP-2-6	SRP-2-7	SRP-2-8	SRP-2-9	SRP-2-13	SRP-2-16	SRP-2-17
SiO ₂	44.32	47.70	47.13	46.87	47.14	46.96	46.06	44.59	46.80	45.91
TiO ₂	2.98	2.81	3.14	3.51	3.20	2.18	3.02	3.01	2.83	3.09
Al ₂ O ₃	12.02	11.78	11.46	11.72	11.47	12.48	11.71	11.68	11.32	10.91
FeO	16.97	13.94	14.05	14.67	14.85	13.52	15.13	17.35	14.65	15.11
MnO	0.20	0.18	0.25	0.21	0.27	0.26	0.24	0.23	0.21	0.31
MgO	11.17	11.19	11.12	10.41	10.86	12.06	10.93	10.60	11.91	12.61
CaO	8.45	7.99	8.80	8.79	8.30	8.52	8.70	7.99	8.20	8.13
Na ₂ O	2.49	2.45	2.42	2.38	2.37	1.97	2.55	2.54	2.01	2.08
K ₂ O	0.74	0.93	0.81	0.79	0.82	1.11	0.72	0.83	0.71	0.73
P ₂ O ₅	0.42	0.72	0.58	0.40	0.44	0.70	0.74	0.65	0.55	0.56
H ₂ O	0.22	0.32	0.24	0.25	0.30	0.25	0.20	0.53	0.81	0.56
olivine FO										
H ₂ O						0.23			0.99	
ppm										
F						977			863	
S						727			927	
Cl						93			77	
Sc	26	25	26	28	27	26	27	24		29
Rb	18.3	22.1	17.9	17.8	17.6	17.4	17.9	19.9		16.5
Sr	275	256	281	275	257	254	265	269		244
Y	37	34	36	40	36	35	35	34		36
Zr	233	252	250	258	242	237	259	222		240
Nb	22.3	23.9	23.2	22.5	21.5	19.3	21.5	21.2		21.4
Ba	442	459	443	442	422	410	444	440		417
La	24.9	26.0	24.9	25.5	25.5	23.8	26.1	24.0		23.0
Ce	66.6	64.1	64.5	65.6	63.8	57.5	67.2	62.1		61.8
Pr	8.2	7.9	8.4	8.5	7.8	7.6	7.6	7.5		7.7
Nd	31.6	33.2	35.3	33.7	31.8	30.4	34.9	30.9		33.0
Sm	7.2	7.9	8.9	7.4	7.5	8.1	7.5	6.3		6.9
Eu	2.8	2.7	3.0	2.9	2.7	2.5	2.3	2.6		2.6

Table 2 continued

wt%	SRP-2-3	SRP-2-4	SRP-2-5	SRP-2-6	SRP-2-7	SRP-2-8	SRP-2-9	SRP-2-13	SRP-2-16	SRP-2-17
Gd	6.7	6.8	8.2	8.0	7.4	7.1	8.3	7.0		8.6
Dy	5.9	7.1	6.7	7.3	6.2	7.3	7.6	6.1		6.0
Er	3.3	3.6	3.7	4.3	4.2	3.3	3.5	2.9		3.6
Yb	3.1	2.9	4.2	2.7	3.5	2.7	3.9	3.2		3.8
Th	2.2	2.6	1.5	2.1	1.8	2.1	2.0	1.2		1.9
U	0.6	0.8	0.7	0.8	0.6	0.5	0.7	0.7		0.7

Major oxides measured using EMPA, H₂O via FT-IR, volatiles (H₂O, F, S, Cl) by SIMS, and trace elements by LA-ICP-MS. Major oxides have been normalized to 100%

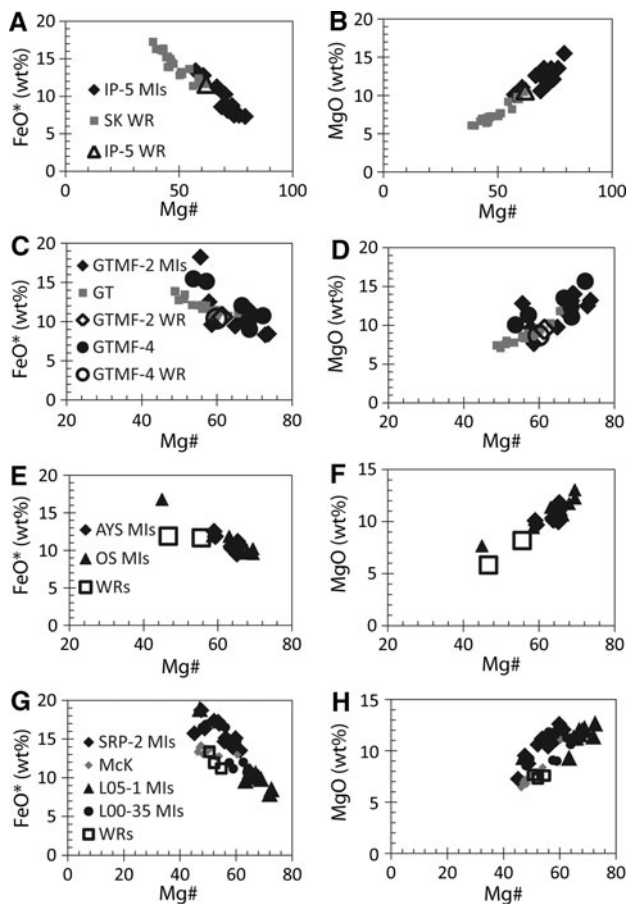


Fig. 3 Plots of FeO and MgO vs. Mg# for studied melt inclusions and host rocks. Compare with data for other local whole rocks from the literature. SK is Spencer-Kilgore lava field (Leeman, unpub. data). GT are Gerrit basalts taken from Christiansen (2001). McK are McKinney basalts from Leeman and Vitaliano (1976). In all these cases, melt inclusions from this study exhibit similar compositional trends to local whole rocks, indicating that melt-inclusion compositions have not been strongly altered by Fe loss or other processes

inclusions found in the sample. Melt inclusions commonly range from less evolved than their host rocks to apparently more evolved (e.g., sample IP-5 has melt inclusions with Na₂O from 1.6 to 5.5 wt%, while the host rock has

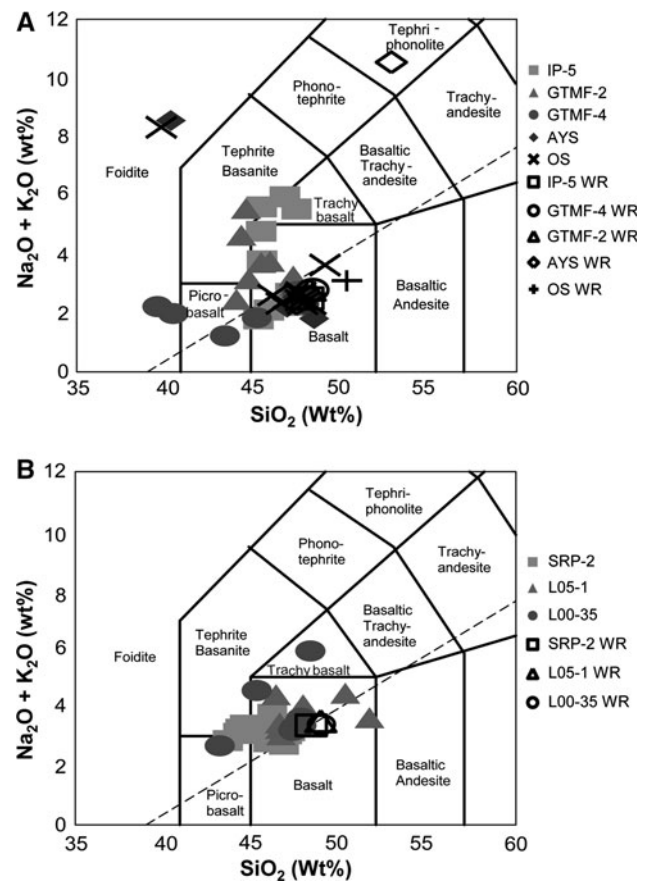


Fig. 4 Total alkalis vs. silica plots for syn-caldera (a) and post-caldera (b) melt inclusions and host rocks (labeled “bulk” in the legend). Syn-caldera melt inclusions show greater heterogeneity, including some with highly alkaline compositions

Na₂O of 2.1 wt%). Also, several samples have inclusions with anomalous compositions not easily related to the rest of the data. For example, each of the samples from Yellowstone (OS and AYS samples) yielded a single inclusion with anomalously high Na₂O (~8 wt%) and low SiO₂ (~40 wt%) (Fig. 5). These inclusions may represent chemical alteration that was not filtered out by

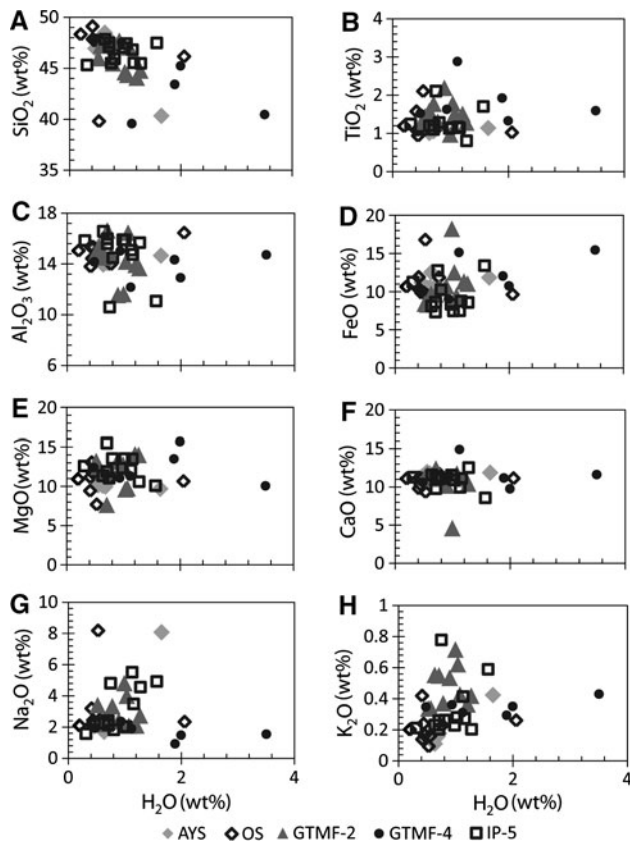


Fig. 5 Harker-style plot of major oxide vs. water concentrations for the studied syn-caldera melt inclusions. Trends are most pronounced for Na_2O and K_2O (g, h) and also demonstrate that water concentrations are generally highest in the least differentiated melt inclusions

inclusion inspection (Nielsen et al. 1998) and therefore should be considered suspect.

Trace-element compositions of the melt inclusions

Most of the inclusions show trace-element patterns that are broadly similar to those of their host rocks, but differences are observed for a few inclusions (Fig. 6). The variability is particularly noticeable in the syn-caldera melt inclusions. This may indicate compositional heterogeneity of the source region or, more likely, represent microenvironments created by crystallization of the magma. Of particular note are some strong enrichments in Ba (>3,000 ppm) for the syn-caldera melt inclusions, often accompanied by a depletion in Th, resulting in very high Ba/Th ratios (500 to >5,000). The anomalous inclusion in Yellowstone sample AYS has one of the more extreme Ba/Th ratios (2573). Many of the host rocks also show elevated Ba/Th ratios, showing that this is a characteristic of these lavas, although extreme ratios in some melt inclusions are probably the result of localized crystallization effects (edge effects).

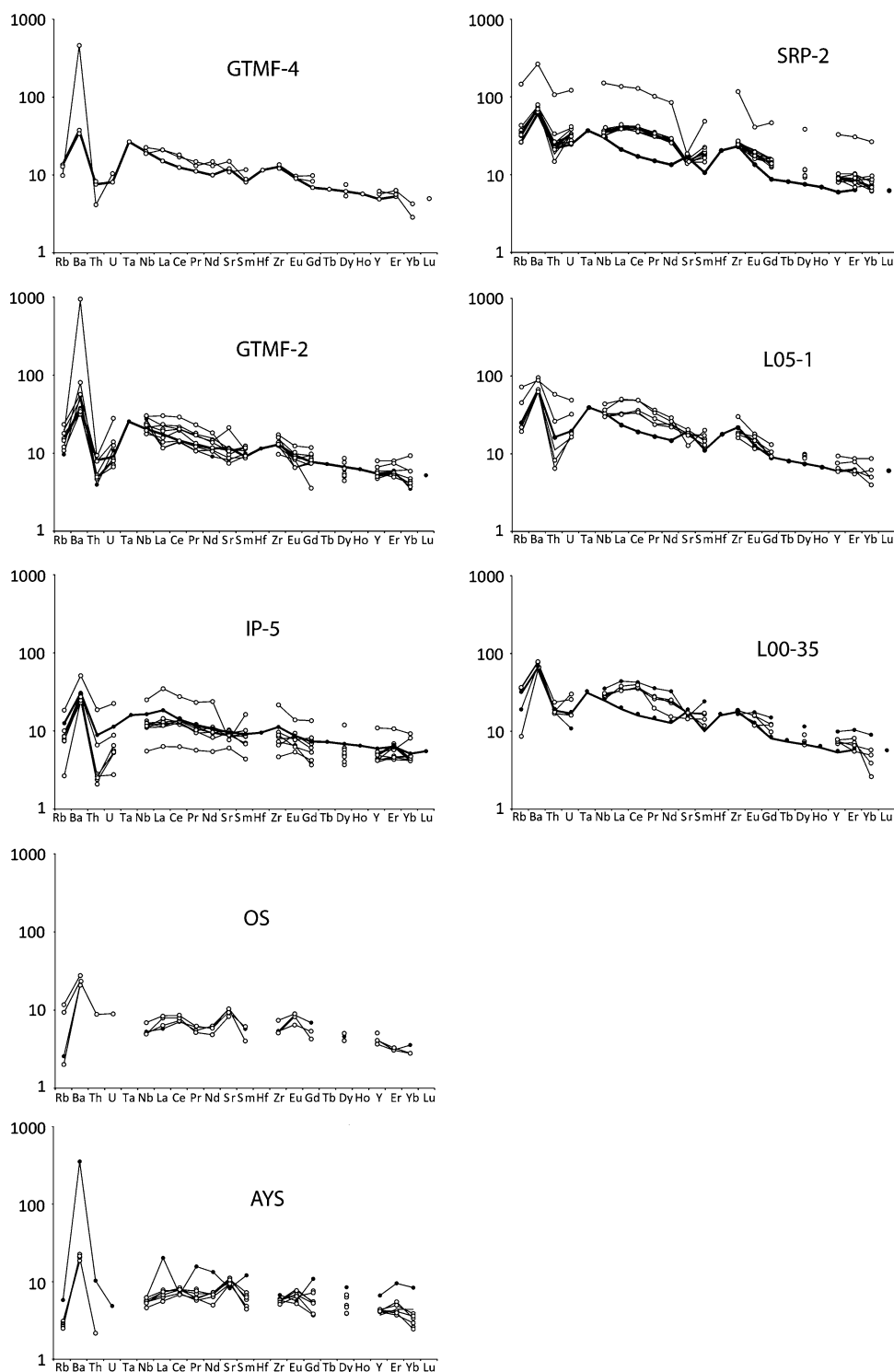
Water in the melt inclusions

Water concentrations in the studied syn-caldera melt inclusions range from 0.3 to 3.3 wt%, with most inclusions showing concentrations <1 wt%. However, all samples have inclusions with ≥ 1 wt% water. The highest water concentrations (>2 wt%) are observed in flows of the Gerritt Basalt from Mesa Falls, Idaho (Fig. 5). More moderate water concentrations are observed in other syn-caldera flows, but all have higher maximum water concentrations than the highest values for post-caldera melt inclusions (Table 2). Some syn-caldera melt inclusions show general trends of increasing Na_2O and/or K_2O with decreasing water concentrations (Fig. 5), indicating that evolved inclusions are probably variably degassed and that the observed concentrations should be interpreted as minima for all inclusions, including those with the highest H_2O concentrations. The most water-rich inclusions tend to be either similar in composition to their host rocks or have less differentiated compositions, increasing confidence that water is not being added by edge effects or alteration. The exception to this is sample AYS, for which the most water-rich inclusion has an anomalous composition, making data from this sample suspect. Furthermore, surface alteration of inclusions would tend to produce inclusion compositions more like the anomalous inclusions in samples AYS and OS (e.g., very high alkalis, very low silica) as opposed to the compositions displayed by other water-rich inclusions in this study. Post-caldera inclusions range from about 0.3 to 0.99 wt% H_2O , with most inclusions having less than 0.6 wt% H_2O . Trends for alkalis vs. H_2O also confirm that more evolved inclusions are variably degassed in the post-caldera inclusions (Fig. 7).

Other volatiles in the melt inclusions

Sulfur concentrations in the syn-caldera melt inclusions range from <300 to 1,700 ppm. Maximum S in the post-caldera melt inclusions, however, was only 968 ppm. Sulfide globules were observed in many inclusions, implying that the values reported here have to be minima for each inclusion analyzed. Chlorine concentrations range from 20 to 1,100 ppm in the syn-caldera inclusions, though most are under 600 ppm, and from <10 to 540 ppm in post-caldera inclusions. Fluorine concentrations ranged from 33 to 689 ppm in the syn-caldera melt inclusions and from 55 to 1,226 ppm in post-caldera inclusions. Fluorine is the only volatile analyzed for which the higher concentrations are observed in the post-caldera melt inclusions and may suggest a crustal contribution possibly from the dissolution of apatite. Fluorine concentrations also show a positive correlation with some

Fig. 6 Trace-element distribution diagrams for host rocks (*continuous lines*) and olivine-hosted melt inclusions for syn-caldera (*left*) and post-caldera (*right*) lavas (*dashed lines*). Note the broad similarity between the inclusions and host rocks, as well as the strong Ba enrichment and Th depletion in some syn-caldera inclusions. Data are normalized to primitive mantle composition from Hoffmann and Welin (1988)



incompatible elements (particularly K_2O) (Fig. 8), indicating that it is not degassing significantly during differentiation. This trend is observed in both syn-caldera and post-caldera melt inclusions. CO_2 was only analyzed in four melt inclusions from sample GTMF-4, ranging from 49.7 to 1,677 ppm.

Discussion

Causes of chemical variability in melt inclusions

There is a great deal of heterogeneity with respect to major oxide, trace-element, and volatile compositions for the

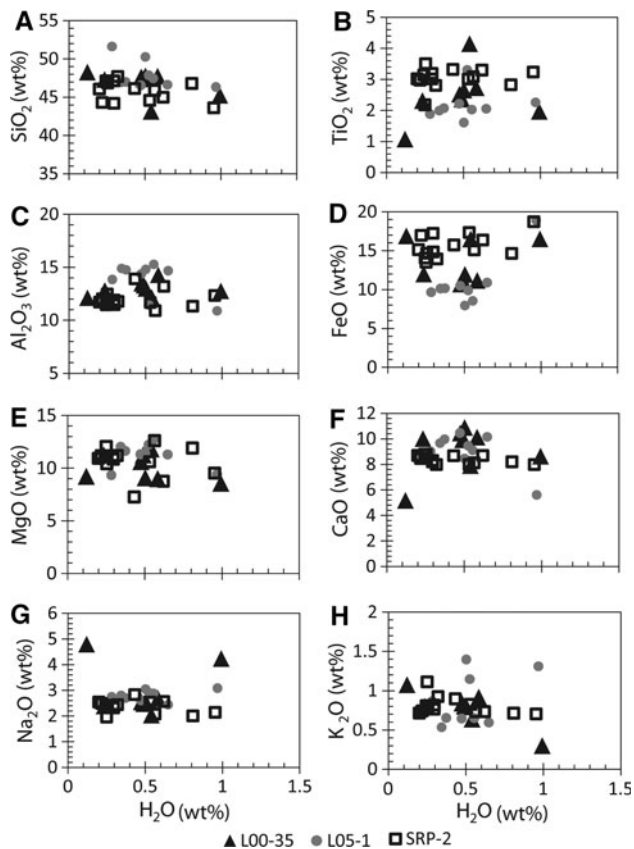


Fig. 7 Harker-style plot of water versus major oxides for the post-caldera melt inclusions. Trends again indicate highest water concentrations in the least differentiated inclusions in these samples

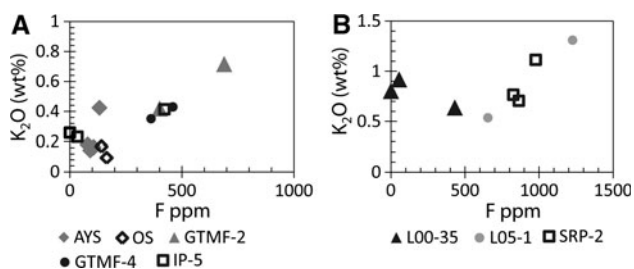


Fig. 8 Plots of K_2O vs. F in syn-caldera (a) and post-caldera (b) melt inclusions. Observed trends indicate quantitative retention of F during differentiation/crystallization

olivine-hosted melt inclusions both in the syn-caldera and post-caldera basalts scattered throughout the eastern Snake River Plain (ESRP). This heterogeneity may result from many factors, as expounded upon in the discussion below. Magmatic degassing may be detectable if it causes crystal growth, which would create trends of decreasing volatile concentrations with increasing concentrations of incompatible elements (Johnson et al. 2008). Fractionation will create commonly observed trends among major oxides, and may also lead to enrichment of volatiles in the residual melt. Another phenomenon, known as the “edge effect”

(discussed in part as localized reaction effects in Danyushevsky et al. (2004), is caused by rapid crystal growth, which exceeds the diffusion rates of some elements and can cause the chemistry of the boundary layer of liquid near a crystal to become somewhat different from the bulk liquid. Zhang et al. (1989), Kress and Ghiorso (1995) and Chen and Zhang (2008) presented data on elemental diffusion rates in basaltic liquids, which have bearing on this process. Because of this edge effect, melt inclusions trapped in this boundary layer may be significantly different from the bulk liquid composition. A sulfide phase can form in trapped sulfur-rich melt inclusions, which primarily influences their composition by removing S from the residual melt inclusion (Danyushevsky et al. 2002). Interaction of the melt inclusion with olivine either soon after entrapment or during homogenization in the laboratory will either add host-olivine components to the inclusion or subtract olivine-compatible components from the inclusion. Post-entrapment degassing of inclusions will only be detected if most inclusions form a trend between a volatile and some major oxide or trace element, in which case, degassed inclusions will plot off the defined trend. This further supports the notion that measured water concentrations for all melt inclusions are minima compared to the actual maximum concentration of the original magma.

Major and trace-element trends: equilibrium crystallization or edge-effect diffusional exchange?

The observed trends between water and incompatible major oxides and trace elements can be explained in part by edge effects occurring immediately prior to entrapment (one type of localized reaction effect discussed by Danyushevsky et al. (2004), which result from rapid crystallization, possibly caused by degassing of water (e.g., Johnson et al. 2008). Some simultaneous enrichment of Al_2O_3 , Na_2O , and K_2O (these three show similar behavior during olivine dissolution, Zhang et al. 1989; Chen and Zhang 2008) is evident. It seems likely that some of the variability in composition of most lower water melt inclusions is due to edge effects. However, even where edge effects were important, water could easily remain in equilibrium with the bulk magma, while incompatible elements shifted to more evolved compositions at the edge of a growing olivine crystal because water has a diffusion rate approximately an order of magnitude greater than most major and trace elements ($\sim 10^{-10} m^2/s$, compared to $\sim 10^{-11} m^2/s$, respectively) (Zhang and Stolper 1991; Chen and Zhang 2008). The fact that in all cases, other than sample AYS, water concentration is highest in less differentiated melt inclusions (which have presumably been the least affected by the edge effect) seems to bear this out.

All of the basalts we have analyzed penetrated continental crust and have compositions that may not have been directly in equilibrium with the mantle, which indicates that they may have experienced some evolution within the crust, potentially including crustal contamination. If crustal contamination occurred at depth, before any crystallization, then melt inclusions would not record it. The scatter about the trends defined by local whole-rock compositions shown in Fig. 3 could be the result of shallow contamination and/or edge effects as described previously. It is also possible that some of the less differentiated compositions that are significantly different from host-rock compositions represent small volume liquids that may have existed in the lower to mid crust and are now only recorded in these melt inclusions. Although this possibility cannot be ruled out, it seems less likely to explain the melt inclusions because some of these inclusions harbor fairly high water concentrations, which, as will be discussed later, would mean that they had to form, be entrained in a normal basaltic magma, and then be transported to the surface in only a few days, a scenario that seems unlikely.

Most major oxides in the syn-caldera basalts show trends with respect to water, despite the scatter. Water concentrations are highest in less differentiated compositions, which appear to be the compositions least effected by edge effects or crustal contamination (Fig. 5). Post-caldera basalts show similar trends in water versus major oxides (Fig. 7). Fluorine behaves differently compared to the other volatiles during evolution of the magma. Fluorine correlates positively with K_2O , which indicates that F is not degassing from magma in a similar manner to the other volatiles (Fig. 8). Sadofsky et al. (2008) also observed similar behavior in F for the Central America Arc. These trends are observed in both syn-caldera and post-caldera basalts, although, again, the correlations are not as well developed in melt inclusions from the post-caldera lavas. Plots of K_2O vs. water for data from Vigouroux et al. (2008) also show this trend in the Mexican arc, and in all cases, the highest water concentrations are only observed in the least differentiated inclusions with respect to incompatible element concentrations.

It is important to note that the high water concentrations preserved in some of the melt-inclusions rule out the possibility of long storage times in the shallow crust for the host magmas. Demouchy and Mackwell (2003) found water diffusion rates through olivine to be $\sim 10^{-13}$ m²/s, which means that water could diffuse through a 1-mm wall of olivine to escape an inclusion in just a few days. Therefore, the observed concentrations support the conclusion that these basalts are not likely to have been stored for very long, at least not after water was degassed. Portnyagin et al. (2008) found that “dry” olivine-hosted melt inclusions placed in a water-bearing

melt could gain up to 2.5 wt% water after only two days at 1,140°C. Although the conditions in the Portnyagin et al. (2008) study are very unlikely to occur in nature (ascent should be characterized by degassing of the host liquid, not addition of water), these experimental results provide further evidence of how quickly water can diffuse in or out of a melt inclusion. Severs et al. (2007) found that melt inclusions in quartz from the Bishop Tuff lost most of their water after only seven days of heating at 800°C and one kbar of pressure. Johnson et al. (2008) examined melt inclusions from various stages of an eruption at Volcan Jorullo, Mexico, and found that early-erupted inclusions preserved high water contents and had very short estimated olivine storage times; later in the eruption, more evolved inclusions were found with much less water and much longer estimated storage times. These reports lend further support to the notion that any amount of storage would cause loss of water in melt inclusions. As soon as host magmas to the melt-inclusion-bearing olivine crystals degas their water, melt inclusions will begin to re-equilibrate with the drier magma and will do so on a scale of days. Therefore, the only way for the high water concentrations observed in a number of the olivine-hosted melt inclusions from the Yellowstone hotspot to be preserved is for eruption to have occurred within a few days following degassing. Hence, it is expected that only a small proportion of inclusions would be able to maintain high H₂O concentrations. This also suggests that much of the crystallization that entrapped those melt inclusions occurred immediately prior to eruption.

Water-fluxed melting?

The association of highest water concentrations with the least differentiated melt inclusions was used by Sadofsky et al. (2008) to argue for water-fluxed melting in arc basalts from Central America. The argument was based on the idea that the addition of water would increase the melt fraction by depressing the peridotite solidus temperature, thereby diluting the concentrations of incompatible elements. High water concentrations in the Yellowstone syn-caldera melt inclusions do not approach arc values, such as those observed by Sadofsky et al. (2008) and others (up to 6 wt%). Furthermore, host-olivine grains in the Central America Arc show much greater heterogeneity in their Fo content than olivine grains in our study (up to 10 wt% compared to only about ± 3 wt% in any given sample from the Yellowstone-SRP volcanic province. Melt inclusions from the ESRP and Yellowstone also vary to compositions that are more evolved than the host rocks, a characteristic not observed in the Central America Arc, which indicates that crystallization effects are more important in the

olivine-hosted melt inclusions from the SRP. Finally, there is little correlation between Ba/La and water in Yellowstone-ESRP rocks, which in the Central American arc setting Sadofsky et al. (2008) considered to be an even more important indicator of water-fluxed melting. It does not seem that water-fluxed melting is an appropriate interpretation for the major- and trace-element trends observed in this study, although it is expected that high water concentrations contributed to melt production during mantle upwelling.

Mantle or crustal source for water and other volatiles

The results presented here suggest that water and other volatiles in the Yellowstone-SRP hotspot track basalts have a deep source. Shallow crystallization immediately prior to and during eruption cannot have enriched water in melt inclusions because it will have degassed at this time, and in fact, melt inclusions with more crystallized compositions have lower, not higher water concentrations. The current dataset does not allow for conclusions to be made as to whether the high water concentrations observed were acquired from the mantle or from mantle melts differentiating in and interacting with the lower crust. However, water concentrations up to 3 wt% in the least evolved basaltic melts of the Yellowstone hotspot are much higher than those in Hawaiian basalts (Hauri 2002). Hence, it is reasonable to state that the hotspot basaltic production in Yellowstone is at least partially due to its hydration. In other words, Yellowstone may also be referred to as a “wet spot”.

Because the highest water values are always observed in the least differentiated melt inclusions (e.g., lowest Na₂O and/or K₂O), it is likely that water was present at depth in abundance—as opposed to being an artifact of shallow differentiation processes. H₂O/Ce ratios plotted versus H₂O (Fig. 9) also indicate that water concentrations are highest when H₂O/Ce is highest in all cases. Cerium has a similar incompatibility to H₂O (Michael 1995) and

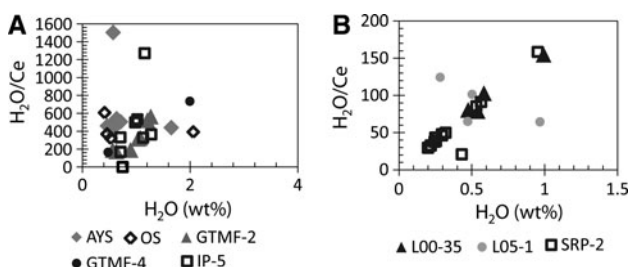


Fig. 9 Plots of H₂O/Ce ratios vs. H₂O in syn-caldera (*left*) and post-caldera (*right*) melt inclusions. The slope indicates that water is being lost by the magma during differentiation

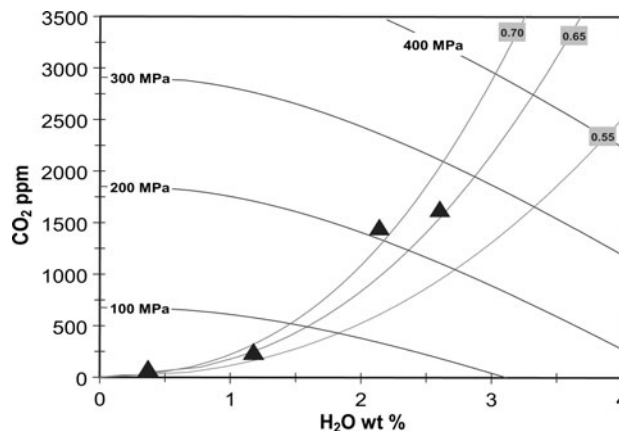


Fig. 10 Plot of CO₂ vs. H₂O concentration for the four melt inclusions from sample GTMF-4. The measured concentrations follow a magmatic degassing curve as determined by Metrich and Wallace (2008)

therefore H₂O/Ce should remain constant during crystallization if no other processes (e.g., degassing) remove water. The highest H₂O/Ce in post-caldera melt inclusions are comparable to values found by Michael (1995) in MORB. Also, the few samples on which CO₂ was measured plot on a magmatic degassing curve (Fig. 10) as determined by Metrich and Wallace (2008), indicating that water and CO₂ are degassing during ascent as recorded by the melt inclusions. On the other hand, the values in syn-caldera melt inclusions are much higher, indicating that water in these inclusions must come from a source more hydrated than the MORB source. Both S and Cl, like water, have their highest abundances in the syn-caldera basalts compared to the post-caldera varieties, although the opposite is true for F. This observation supports the notion that volatiles are coming from a residual source in the mantle or crust that can be depleted by melting. For comparison, maximum Cl values observed in basalts from the Central America Arc (Sadofsky et al. 2008) reach 2,275 ppm, while in Hawaii (Hauri 2002), values only reach 435 ppm (for Loihi volcano). Chlorine concentrations in the SRP are intermediate between these two; note, however, that the minimum concentrations observed in the SRP are much lower than those reported for either of the comparison localities, indicating that the post-caldera inclusions are significantly degassed with respect to Cl, if the source is otherwise similar to those in plumes or arcs. The higher Cl concentrations favor a more arc-like source, or at least a component of such a source, rather than a Hawaii-type plume. Maximum S concentrations observed in both Hawaii and the Central America Arc are similar (~2,200–3,000 ppm and ~2,400 ppm, respectively), and SRP melt inclusions also fall in this range.

Ba and Th evidence for subduction-related fluids in melt inclusions

Ba enrichments are observed in inclusions and host rocks from four of the five syn-caldera lava samples. These enrichments are the most prominent feature of the trace-element patterns (Fig. 6) for some of the syn-caldera melt inclusions and host rocks. They are observed in both Gerrit Basalt samples, and in both cases, the melt inclusions are otherwise very similar to their host rocks in composition. Although the strongest Ba enrichments are likely enhanced by edge effects, the presence of high Ba and Ba/Th in host rocks indicates that this is a robust characteristic of the source components. The fifth of the syn-caldera samples from Yellowstone also shows this Ba enrichment (AYS-4). However, this inclusion has noticeably different major oxide and trace-element compositions compared to the other inclusions in this population and is therefore considered suspect. Most significantly, it has anomalously high Na_2O and low SiO_2 (Table 2; Figs. 4, 5). It also has a much higher water concentration than the other inclusions from this rock. However, its host-olivine Fo value falls in the range defined by the other olivine grains from this rock, suggesting that the grain with the anomalous melt inclusion is not likely to be xenocrystic. We therefore view the high water concentration in this inclusion with some caution as it might have been influenced by crystallization processes and not just the melt source characteristics.

Thorium depletion in melt inclusions is observed in four of the five syn-caldera lavas, and is particularly pronounced in the suite of inclusions from sample IP-5 (Fig. 6). The melt inclusions from this rock show wider compositional scatter both in major oxides and trace elements than do inclusions from the other rocks (Fig. 5; Table 2), suggesting either that its source was more heterogeneous and/or that its precursor magma experienced a higher degree of differentiation/crustal contamination. The latter possibility may be supported by the presence of flows in this field of more evolved basalts where olivine is absent and large plagioclase crystals are the only phenocrysts. Most of the melt inclusions from sample IP-5 do not show much Ba enrichment relative to the whole rock but these inclusions do show a very pronounced depletion in Th. While no significant Ba enrichment in the melt inclusions relative to host rocks was observed for post-caldera basalts, some of the melt inclusions do have small Th depletions.

To understand the origins of the melt-inclusion trace-element characteristics, plots of Ba/La vs. Ba/Nb and Ba/Th vs. Rb/Nb have been prepared (Fig. 11) and compared to similar diagrams by Weaver (1991) who defined some mantle end members using the same trace-element space. In the plot of Ba/La vs. Ba/Nb (Fig. 11a), the mantle end members plot on a mixing line between average

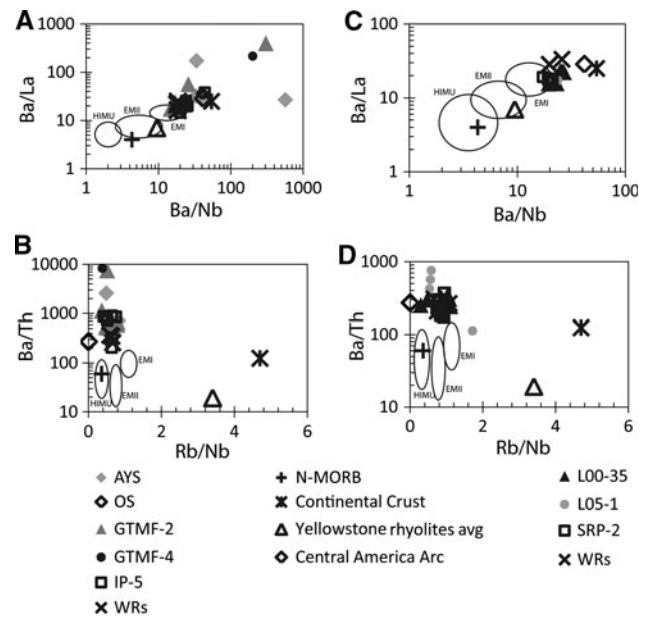


Fig. 11 Plots of Ba/La vs. Ba/Nb and Ba/Th vs. Rb/Nb for syn-caldera melt inclusions and host rocks (*left*; **a**, **b**) and post-caldera melt inclusions and their host rocks (*right*; **c**, **d**). Also included are estimated compositions for N-MORB, continental crust from Weaver (1991), Yellowstone rhyolites from Christiansen (2001) and an average for the Central America Arc from Sadofsky et al. (2008) (they did not analyze Rb, so the Ba/Th ratios are plotted on the axis). The fields for the mantle end members are from Weaver (1991). Note that many inclusions plot away from the fields denoted by the mantle end members, instead exhibiting compositions normally seen in arcs

primitive mantle and average continental crust. Melt inclusions and host rocks from the SRP define a parallel line slightly above that particular mixing line but with a few points much higher, representing the strongly Ba-enriched melt inclusions. Similar patterns emerge on the Ba/Th vs. Rb/Nb diagram (Fig. 11b), where melt inclusions define a near-vertical trend for both syn-caldera and post-caldera basalts. In the syn-caldera basalts, whole rocks also plot above the trend, though extreme compositions occur only in a few of the melt inclusions (again this is probably the result of diffusional enhancement by the edge effect). Comparing our results on basaltic rocks to data published by Christiansen (2001) for Yellowstone Caldera rhyolites shows contrasting trace-element patterns that are not explicable by simple processes, such as extreme crystal fractionation, demonstrating that contamination by components in those rhyolites probably did not play a role in producing the observed patterns in our melt inclusions. High Ba/Th ratios and Ba concentrations typify arc basalts as a result of the strong difference in mobility within fluids for these two elements. The Yellowstone-SRP samples display patterns similar to those observed in arcs (Walker et al. 2003; Churikova et al. 2007; Sadofsky et al. 2008). The fact that similar patterns are observed in the syn-caldera basalts at Yellowstone suggests that arc or

subduction-related components may be present in the source of the Yellowstone-SRP magmas.

Possible source of water and volatiles in the Mantle/Crust

Yellowstone and the SRP are significantly enriched in volatiles when compared with Hawaii, a typical hotspot. Maximum water concentrations in all but one of the sampled rocks—including both syn-caldera and post-caldera samples (0.8–3.5 wt%)—exceed the maximum concentrations observed in Hawaii of 0.8–0.9 wt% (Hauri 2002), by more than a factor of three if we focus on the maximum values in each case. We reiterate that syn-caldera samples have the highest measured water concentrations (up to 3.3 wt% H₂O). Although the basalts may have acquired their high water contents in the crust, the studied Yellowstone-SRP appears to be significantly more hydrated than Hawaii. Furthermore, the Yellowstone-SRP magmatic province contains a component that appears to resemble the arc source. This evidence suggests that the water may not have come from the hypothesized plume but instead was left behind in the mantle or crust during a previous subduction event and was then either mixed with the rising plume or the plume simply supplied the heat that melted some subduction-fluxed components residing in the upper mantle or lower crust.

Alternatively, an argument could be made that the plume source harbors subducted components as has been argued by others for a few decades in the case of ocean islands (e.g., White and Hofmann 1982; White 1985; Hofmann et al. 1986). However, this argument is unsatisfying as an explanation of the high water abundances in the Yellowstone-SRP melt inclusions because volatiles should be mostly lost by the subducted slab long before its materials can be incorporated into a mantle plume at great depth. Direct participation of such a source cannot be completely ruled out, but seems inadequate to explain the nearly arc-like water concentrations observed.

If we accept a subduction-related origin for the water reported here, then the most likely source for it beneath Yellowstone and the SRP is the Farallon slab, thought to be responsible for the Absaroka arc just east of Yellowstone, and other older volcanism in the Northwestern United States (Feeley 2003). It is reasonable to infer that all water released by the Farallon slab was not removed from the lithospheric mantle or lower crust by contemporaneous melting; some residual water was left behind, perhaps in hydrous-phase-bearing veins (cf. Foley 1992) that were also enriched in Ba and depleted in Th. This material then melted when the hypothesized plume impinged upon the lithosphere and introduced a thermal anomaly into the upper mantle. Melts produced in the lithospheric mantle

may then have been contaminated by a plume component—if reported ³He/⁴He values of ~16 R/R_A values in the SRP (Craig et al. 1978; Graham et al. 2009) are representative of the mixing that impacted the principal components in the magmas. The post-caldera melts have lower water concentrations, as they sample a mantle and crust that had undergone melting just a few million years before, during syn-caldera volcanism, and would likely have lost much of their water during that first phase of melting.

Alternatively, Leeman et al. (2009) note isotopic evidence for Archean metasomatism of the SRP lithosphere; therefore, it is possible that the water in SRP melts is residual to that event. While we cannot rule out this possibility, it seems less likely, considering the high probability that water would have been removed by earlier melting events during this region's long and complex history of tectonic and volcanic activity.

Conclusions

Our measurements of major oxide, trace-element, and volatile [H₂O, S, F, and Cl] concentrations in melt inclusions from eight basalt samples representing both syn-caldera and post-caldera phases of melting along the Yellowstone-SRP hotspot track demonstrate high concentrations of H₂O and other volatiles in the mantle or lower crust. The results have been compared with data obtained from the host rocks, as well as data from the literature for other plume-related volcanic provinces to make interpretations on the development of observed trends and also on the sources of the detected volatiles.

Many melt inclusions have significant concentrations of water and other volatiles. Observed water and other volatile concentrations are higher in the syn-caldera basalts than in their post-caldera counterparts, with the exception of F. A significant fraction of the melt inclusions studied have low-volatile concentrations—likely due to degassing—underlining the importance of analyzing many inclusions thereby ensuring that at least a few inclusions with the maximum volatile concentrations are found. Overall, the concentrations we have reported here for the syn-caldera melt inclusions are higher than those observed in Hawaii (up to 3.3 wt% for Y-SRP vs. 0.9 wt% for Hawaii), but generally lower than the values observed in many arcs (6 wt% or more). Post-caldera melt inclusions have generally lower volatile concentrations, potentially indicating that residual hydration in the upper mantle or lower crust was largely consumed during the first phase of melting during and immediately after the caldera-forming eruptive events, in many cases, several million years before the second phase of melting along the SRP that is attributed to Basin and Range extension.

Trends observed between volatiles (with the exception of F) and certain major oxides and trace elements indicate that the highest volatile concentrations are associated with the least differentiated melt inclusions, suggesting a deep, mantle, or lower crustal source for the volatiles. These trends also suggest considerable degassing of the volatiles from the basalts immediately prior to eruption, ruling out shallow volatile enrichment as a result of edge effects or shallow crustal interaction. High Ba concentrations, as well as Ba/La and Ba/Th ratios observed in some melt inclusions and host rocks may be consistent with the presence of an arc-related signature. This suggests that volatiles existed as residual hydration of the upper mantle resulting from the subduction of the Farralon slab or some other previous subduction event. The hydration state of the lithosphere beneath the Yellowstone-SRP magmatic province allows for significant melting even if the hypothesized plume is not particularly hot. The impingement of this plume upon these hydrated domains triggered the melting that produced the water-rich and incompatible-element-enriched basalts observed at Yellowstone and the Snake River Plain.

Acknowledgments The authors thank all individuals at laboratories at the University of Michigan and other institutions who provided essential support with instrumentation in the process of data acquisition for this study. Shaul Hurwitz of USGS provided splits of olivine samples from Yellowstone National Park, and Yellowstone NP provided us permission to work on them. Several people read the manuscript and provided valuable input to which we are indebted, particularly Youxue Zhang, Becky Lange and Sarah Rilling. We would also like to thank the editor and CMP reviewers L. Danyushevsky and an anonymous reviewer for their thoughtful comments, which have further enriched this paper. Leeman acknowledges support of the National Science Foundation for providing time and resources to allow his involvement. This work was supported by NSF grant EAR-0911353 S. Mukasa.

References

- Bonnichsen B, Leeman WP et al (2008) Miocene silicic volcanism in southwestern Idaho: geochronology, geochemistry, and evolution of the central Snake River Plain. *Bull Volcanol* 70(3):315–342
- Camp VE (1995) Mid-miocene propagation of the yellowstone mantle plume head beneath the Columbia River Basalt source region. *Geology* 23(5):435–438
- Camp VE, Ross ME (2004) Mantle dynamics and genesis of mafic magmatism in the intermontane Pacific Northwest. *J Geophys Res Solid Earth* 109(B8)
- Carlson RW (1984) Isotopic constraints on Columbia River Flood-Basalt Genesis and the Nature of the Subcontinental Mantle. *Geochim Cosmochim Acta* 48(11):2357–2372
- Castro MC, Ma L et al (2009) A primordial, solar He-Ne signature in crustal fluids of a stable continental region. *Earth Planet Sci Lett* 279(3–4):174–184
- Chen Y, Zhang Y (2008) Olivine dissolution in basaltic melt. *Geochim Cosmochim Acta* 72(19):4756–4777
- Christiansen RL (2001) The quaternary and Pliocene Yellowstone Plateau volcanic field of Wyoming, Idaho, and Montana
- Christiansen RL, Foulger GR et al (2002) Upper-mantle origin of the Yellowstone hotspot. *Geol Soc Am Bull* 114(10):1245–1256
- Churikova T, Worner G et al (2007) Volatile (S, Cl and F) and fluid mobile trace element compositions in melt inclusions: implications for variable fluid sources across the Kamchatka arc. *Contrib Mineral Petrol* 154(2):217–239
- Craig H (1993) Yellowstone hotspot; a continental mantle plume. *Eos Trans Am Geophys Union* 74:602
- Craig H, Lupton JE et al (1978) Helium isotope ratios in Yellowstone Park and Lassen Park Volcanic gases. *Geophys Res Lett* 5(11):897–900
- Danyushevsky LV, McNeill AW et al (2002) Experimental and petrological studies of melt inclusions in phenocrysts from mantle-derived magmas: an overview of techniques, advantages and complications. *Chem Geol* 183(1–4):5–24
- Danyushevsky LV, Leslie RAJ et al (2004) Melt inclusions in primitive olivine phenocrysts: the role of localized reaction processes in the origin of anomalous compositions. *J Petrol* 45(12):2531–2553
- Demouchy S, Mackwell S (2003) Water diffusion in synthetic iron-free forsterite. *Phys Chem Minerals* 30(8):486–494
- Dixon JE, Stolper EM et al (1995) An experimental study of water and carbon dioxide solubilities in mid ocean ridge basaltic liquids. 1. Calibration and solubility models. *J Petrol* 36(6):1607–1631
- Feeley TC (2003) Origin and tectonic implications of across-strike geochemical variations in the Eocene Absaroka volcanic province, United States. *J Geol* 111(3):329–346
- Foley S (1992) Vein-Plus-Wall-Rock melting mechanisms in the lithosphere and the origin of Potassic Alkaline Magmas. *Lithos* 28(3–6):435–453
- Geist D, Richards M (1993) Origin of the Columbia Plateau and Snake River plain: deflection of the Yellowstone plume. *Geology* 21(9):789–792
- Graham DW, Reid MR, Jordan BT, Grunder AL, Leeman WP, Lupton JE (2009) Mantle source provinces beneath the Northwestern USA delimited by Helium Isotopes in Young Basalts. *J Volcanol Geotherm Res* 188(1–3):128–140
- Gripp AE, Gordon RG (2002) Young tracks of hotspots and current plate velocities. *Geophys J Int* 150(2):321–361
- Harry DL, Leeman WP (1995) Partial melting of melt metasomatized subcontinental Mantle and the Magma source potential of the lower lithosphere. *J Geophys Res Solid Earth* 100(B6):10255–10269
- Hart WK (1985) Chemical and isotopic evidence for mixing between depleted and enriched Mantle, Northwestern USA. *Geochim Cosmochim Acta* 49(1):131–144
- Hauri E (2002) SIMS analysis of volatiles in silicate glasses, 2: isotopes and abundances in Hawaiian melt inclusions. *Chem Geol* 183(1–4):115–141
- Hildreth W, Halliday AN et al (1991) Isotopic and chemical evidence concerning the genesis and contamination of Basaltic and Rhyolitic Magma Beneath the Yellowstone Plateau volcanic field. *J Petrol* 32(1):63–138
- Hofmann AW, Welin E (1988) Chemical differentiation of the earth; the relationship between mantle, continental crust, and oceanic crust. *Earth Planet Sci Lett* 90(3):297–314
- Hofmann AW, Jochum KP et al (1986) Nb and Pb in Oceanic Basalts—new Constraints on Mantle evolution. *Earth Planet Sci Lett* 79(1–2):33–45
- Hui HJ, Zhang YX et al (2008) Pressure dependence of the speciation of dissolved water in rhyolitic melts. *Geochim Cosmochim Acta* 72(13):3229–3240

- Johnson DM, Hooper PR, Conrey RM (1999) GeoAnalytical Lab, Washington State University. *Adv X-ray Anal* 41:843–867
- Johnson ER, Wallace PJ et al (2008) Magmatic volatile contents and degassing-induced crystallization at Volcan Jorullo, Mexico: implications for melt evolution and the plumbing systems of monogenetic volcanoes. *Earth Planet Sci Lett* 269(3–4):477–486
- Jordan BT, Grunder AL et al. (2004) Geochronology of age-progressive volcanism of the Oregon High Lava Plains: Implications for the plume interpretation of Yellowstone. *J Geophys Res Solid Earth* 109(B10)
- Kent AJR (2008) Melt inclusion in basaltic and related volcanic rocks. *Rev Mineral Geochem* 69(1):273–331
- Kent AJR, Stolper EM et al. (2004) Mantle heterogeneity during the formation of the North Atlantic Igneous Province: constraints from trace element and Sr-Nd-Os-O isotope systematics of Baffin Island picrites. *Geochem Geophys Geosyst* 5
- Knaack C, Cornelius S, Hooper PR (1994) Trace element analysis of rocks and minerals by ICP-MS. Open File Report. Department of Geology, Washington State University, Washington
- Kovalenko VI, Naumov VB et al (2007) Volatiles in basaltic magmas of ocean islands and their mantle sources: I. Melt compositions deduced from melt inclusions and glasses in the rocks. *Geochem Int* 45(2):105–122
- Kress VC, Ghiorso MS (1995) Multicomponent diffusion in basaltic melts. *Geochem Cosmochim Acta* 59(2):313–324
- Le Voyer M (2008) Two contrasting volatile element compositions in primary melt inclusions from Mount Shasta. *Eos* 89(53, Suppl):V31B–2132
- Leeman WP (1982) Development of the Snake River plain-Yellowstone Plateau Province, Idaho and Wyoming; an overview and petrologic model. *Bull Idaho Bureau Mines Geol* 26:155–177
- Leeman WP, Vitaliano CJ (1976) Petrology of McKinney Basalt, Snake River Plain, Idaho. *Geol Soc Am Bull* 87(12):1777–1792
- Leeman WP, Annen C et al (2008) Snake River plain-Yellowstone silicic volcanism; implications for magma genesis and magma fluxes. *Geol Soc Sp Publ* 304:235–259
- Leeman WP, Schutt DL, Hughes SS (2009) Thermal structure beneath the Snake River Plain: implications for the Yellowstone hot spot. *J Volcanol Geotherm Res* 188(1–3):128–140
- Luhr JF (2001) Glass inclusions and melt volatile contents at Paricutin Volcano, Mexico. *Contrib Mineral Petrol* 142(3): 261–283
- Manea VC, Manea M, Leeman WP, Schutt DL (2009) The influence of plume head-lithosphere interaction on magmatism associated with the Yellowstone hotspot track. *J Volcanol Geotherm Res* 188(1–3):68–85
- McCurry M, Rogers DW (2009) Mass transfer along the Yellowstone hotspot track I: Petrologic constraints on the volume of mantle-derived magma. *J Volcanol Geotherm Res* 188(1–3):86–98
- Metrich N, Wallace PJ (2008) Volatile Abundances in Basaltic Magmas and their Degassing Paths Tracked by Melt Inclusions. *Minerals, Inclusions and Volcanic Processes*. Putirka KD, Tepley FJ 69: 363–402
- Michael P (1995) Regionally Distinctive sources of depleted Morb—evidence from trace-elements and H₂O. *Earth Planet Sci Lett* 131(3–4):301–320
- Moore G, Vennemann T et al (1998) An empirical model for the solubility of H₂O in magmas to 3 kilobars. *Am Mineral* 83(1–2):36–42
- Nash BP, Perkins ME et al (2006) The Yellowstone hotspot in space and time: Nd and Hf isotopes in silicic magmas. *Earth Planet Sci Lett* 247(1–2):143–156
- Nielsen RL, Michael PJ et al (1998) Chemical and physical indicators of compromised melt inclusions. *Geochem Cosmochim Acta* 62(5):831–839
- Pierce KL, Morgan LA (1992) The track of the Yellowstone hot spot; volcanism, faulting, and uplift. *Memoir Geol Soc Am* 179:1–53
- Portnyagin M, Almeev R et al (2008) Experimental evidence for rapid water exchange between melt inclusions in olivine and host magma. *Earth Planet Sci Lett* 272(3–4):541–552
- Sadofsky SJ, Portnyagin M et al (2008) Subduction cycling of volatiles and trace elements through the Central American volcanic arc: evidence from melt inclusions. *Contrib Mineral Petrol* 155(4):433–456
- Severs MJ, Azbej T et al (2007) Experimental determination of H₂O loss from melt inclusions during laboratory heating: evidence from Raman spectroscopy. *Chem Geol* 237(3–4):358–371
- Shervais JW, Vetter SK et al (2006) Layered mafic sill complex beneath the eastern Snake River Plain: evidence from cyclic geochemical variations in basalt. *Geology* 34(5):365–368
- Thompson RN (1975) Primary Basalts and Magma Genesis in the Snake River Plain, Idaho, USA. *Contrib Mineral Petrol* 52(3):213–232
- Vigouroux N, Wallace PJ et al (2008) Volatiles in high-K magmas from the western Trans-Mexican volcanic belt: evidence for fluid fluxing and extreme enrichment of the mantle wedge by subduction processes. *J Petrol* 49(9):1589–1618
- Walker JA, Roggensack K et al (2003) The water and trace element contents of melt inclusions across an active subduction zone. *Contrib Mineral Petrol* 146(1):62–77
- Wallace PJ (2005) Volatiles in subduction zone magmas: concentrations and fluxes based on melt inclusion and volcanic gas data. *J Volcanol Geotherm Res* 140(1–3):217–240
- Weaver BL (1991) The origin of Ocean Island Basalt End-Member compositions—trace-element and isotopic constraints. *Earth Planet Sci Lett* 104(2–4):381–397
- White WM (1985) Sources of Oceanic Basalts—radiogenic isotopic evidence. *Geology* 13(2):115–118
- White WM, Hofmann AW (1982) Sr and Nd Isotope geochemistry of Oceanic Basalts and Mantle evolution. *Nature* 296(5860):821–825
- Yuan HY, Dueker K (2005) Teleseismic P-wave tomogram of the Yellowstone plume. *Geophys Res Lett* 32(7)
- Zhang YX, Stolper EM (1991) Water diffusion in a Basaltic Melt. *Nature* 351(6324):306–309
- Zhang YX, Walker D et al (1989) Diffusive crystal dissolution. *Contrib Mineral Petrol* 102(4):492–513